TIA Topologies used in CMOS-MEMS Resonators: A Detailed Review

Vanita [a], Suresh Kumar [a], Ashish Kumar Luhach [b]

[a] *Maharishi Dayanand University, Rohtak, Haryana, India*
[b] *Papua New Guinea University of Technology, Papua New Guinea*

Abstract

In the field of wearables implants use of CMOS-MEMS resonators in sensing applications make a revolutionization due to their miniaturizing capabilities. They are used as frequency deciding elements in an oscillator circuit used in radiofrequency range. The sensed signals are amplified using front end TIAs integrated with the structure itself. It also results in durability of the device used due to low power consumption. The on-chip TIA integration along with CMOS-MEMS structure gives a compact circuit and also helps in amplifying the weak signals sensed by the electrodes of the sensors. The use of LDC helps in converting the analog signals into digital ones. Due to microfabrication techniques involved these MEMS structures are used in various applications including healthcare as sensors, in oscillators for timing, in filters for frequency selection etc. This review work gives an insight about various TIA topologies used in CMOS-MEMS resonators. It also includes a comparative analysis of the various research works giving an insight of the future development.

Keywords

CMOS-MEMS, Front-end TIAs, Sensors, LDC, Amplifier, Gain Bandwidth

1. Introduction

Trans-impedance amplifiers plays an important role in biomedical sensors as they are used with photodiodes which converts the incoming optical signals into current signals as shown in figure 1, which ultimately changed into respective voltage signals using the TIA [1-2]. These amplified voltage signals are fed to either analog to digital converters or any other processor according to the specific application. Biomedical sensors which employ optical fibers have the function of acceptor and converter with features like sensitivity, accuracy, linearity, reproducibility, wide range, precision, quick response time, lower manufacturing cost etc. These optical fibre sensing systems focused on high integration, to reduce the size and consumption of power, eventually moving from discrete components towards on chip implementations [3].

Mainly wearable blood pressure instruments which are under development are based on PPG (Photo Plethysmo Graphy) or PTT (Pulse Transit Time) techniques, thus require no medical supervision. They are low cost and comfortable to use but needs improvement in terms of accuracy and calibration. The main features of wearables devices include long battery life which is possible due to moderate power consumption along with high reconfigurability to readout signals from different measurement locations and conditions [4-5]. Recently, LDC (light to digital converter) are used frequently in biomedical optical sensor readout, so as to directly change the light into usable data. LDCs are used to convert light signals from any light source like LED into electrical signals using photodiode. Basically, a LDC has an integrator for sampling, a current to voltage converter and a filter

WCES-2022: Workshop on Control and Embedded Systems, April 22 – 24, 2022, Chennai, India.
EMAIL: vanita.ece57@gmail.com (Vanita)
ORCID: 0000-0003-0564-4879 (Vanita)

together, which is accompanied by a variable comparator and a counter, converting integrator output directly into a digital code [6-8].

Different design techniques are used in fabricating the TIAs keeping in mind various factors such as size, power consumption, input impedance, bandwidth range, trans-impedance gain, cost etc. The main emphasis is on using microwave components resulting into miniaturization and reduced power consumption which helps in prolonged battery life along with wide dynamic range covering different types of signals. TIAs having fixed trans-impedance gain are not suitable to be used in a wide dynamic range. The dynamic range of a TIA depends on its overload current and sensitivity [9].

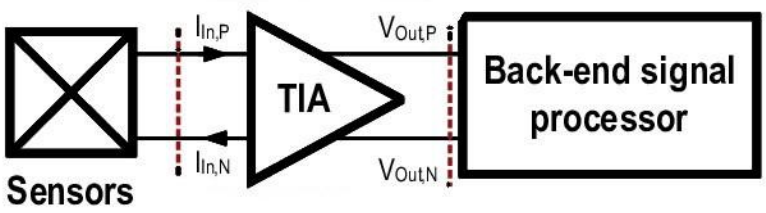

Figure 1: On-chip TIA used in bio-medicals as sensors

Microwave components like power splitters/combiners, filters, couplers, diplexers, resonators are frequently used now-a-days to replace the conventional practice of connecting individually microwave circuits in RF and sensing applications. This approach results into compact systems with improved performance. Here the size reduction is possible using different ways such as by removing all the discrete matching circuits, by integrating filters with other components, by removing splitting networks and by integrating non-linear or active circuits.

On considering resonators whose type depends upon the system requirement including size, insertion loss, bandwidth achieved, power and cost etc, CMOS-MEMS resonator/oscillator along with TIA results in integrated miniaturized structures which is a prerequisite in case of wearable sensors with low power consumption [10].

In this paper starting with on-chip trans-impedance amplifiers used in biomedical applications as sensors, section 2 includes CMOS-MEMS oscillators and section 3 gives various front end TIAs used in these with their parameters and section 4 is about recent developments and a comparative analysis of the reported work. The section 5 gives a glimpse of scope of future research work in this field and finally the paper is concluded in section 6.

2. CMOS-MEMS Oscillator

In order to discuss about integrating various components on a single chip, so CMOS-MEMS technology provide the solution in this direction. In this technology, various interfacing circuits such as sensors, actuators, oscillators are fabricated on a single chip. They help in making portable sensing nodes especially in bio-medicals, giving timely information. It is also possible to combine these structures with application specific customized integrated circuits. These combinations are possible using two methods, namely SIP (System in package) and SoC (System on chip). In SIP various mechanical components and MEMS structure are interfaced using chip or wafer level bonding. In SoC both the structures including MEMS and application specific are monolithically integrated on the same substrate by fabricating [11].

For generation of desired frequency, CMOS-MEMS Oscillator/Resonator is used in closed loop with TIA in series. In contrast to high value of dynamic impedance present in crystal oscillators due to parallel resonance present in them, these CMOS-MEMS Oscillators works on series resonance with TIA. They have three stages as shown in figure 2, first stage is of current to voltage converter, second is of phase compensator and last is of amplifier [12]. MEMS structures are classified in three

categories based on the materials used. They are back end of line metal layers, polysilicon layers and stack of metal layers and silicon dioxide. Different etching methods are used for their fabrication [13].

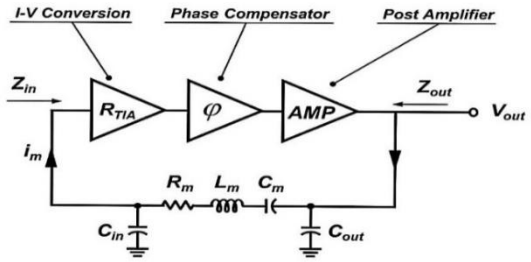

Figure 2: CMOS-MEMS Oscillator

In order to get the desired frequency, the TIA gain is kept higher than the impedance of the oscillator. So, to achieve the gain bandwidth product the third stage of voltage amplification is added. Here the TIA used depends on the frequency of resonator.

3. Front END TIAs

Various front end TIAs used with such resonators are explained in subsequent paragraphs.

3.1. TIA with buffer and resistor as load

It is the simplest one as shown in figure 3, but there is a trade-off between gain bandwidth products here. To overcome its drawback, feedback is added. The negative feedback added here results in stability and increase in bandwidth range in the verge of gain reduction [14]. Its parameters are given by:

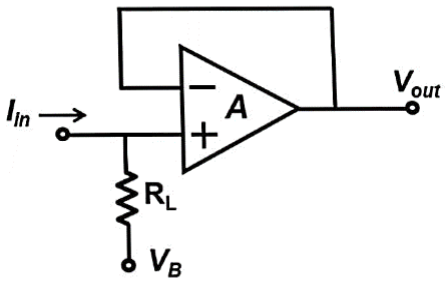

Figure 3: TIA with buffer and resistor as load

- Trans-impedance Gain $G = R_L$ where R_L is the load resistance.
- Bandwidth $BW = \frac{1}{R_L C_P}$ where Cp is the photodiode capacitance.
- Input referred noise current $\frac{4k_B T}{R_L} + \frac{v_n^2}{\Delta f}\omega^2 C_P^2$ where k_B is Boltzmann's constant, T is temperature, ω is angular frequency and v_n^2 is output voltage noise.

3.2. TIA with Negative Feedback

In this shunt resistor and capacitor feedback is added on negative terminal of op-amp as shown in figure 4. As a result, TIA gain over a wider bandwidth is achieved [15]. The feedback resistor Rf with a parallel capacitive feedback CF sets the gain and frequency response.

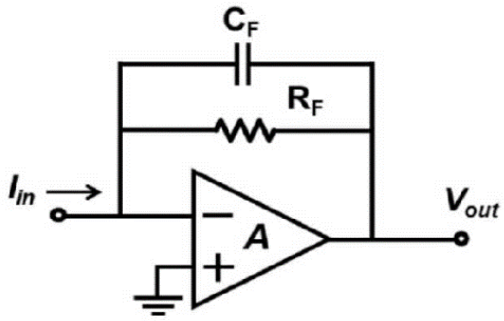

Figure 4: TIA with negative feedback

(for $R_f << R_b$)

- TIA Gain $G = R_F$
- Input referred noise current $\frac{4k_BT}{R_L} + \frac{v_n^2}{\Delta f}\left(\frac{1}{R_F^2} + \omega^2(C_P + C_F)^2\right)$

(for $R_f \rightarrow R_b$)

- TIA Gain $G = \frac{1}{\omega C_F}$ where C_F is feedback capacitor
- Input referred noise current $\frac{4k_BT}{R_B} + \frac{v_n^2}{\Delta f}\left(\frac{1}{R_B^2} + \omega^2(C_P + C_F)^2\right)$

3.3. TIA as current amplifier

Here FETs are used as shown in figure 5 which gives lesser input impedance values, improving gain further but on the sake of noise performance Here transistors used as feedback resistor to minimize the output ripple and omit the extra drawn current. Bandwidth of TIA increases by decreasing the photodetector capacitance (~1pF). In order to boost the voltage swing and match the output impedance to drive the photo-receiver output [16].

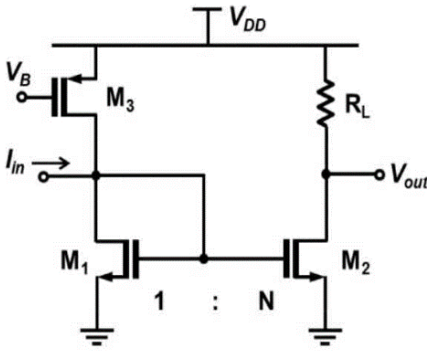

Figure 5: TIA as current amplifier

- Gain $G = NR_L$
- Bandwidth $BW = \frac{1}{g_{m1}C_P}$ where g_{m1} is the trans-conductance
- Input referred noise current $4k_BT\Upsilon(g_{m1} + g_{m3}) + 4k_BT\left(\Upsilon g_{m2} + \frac{1}{R_2}\right)\frac{1}{N^2}$ where Υ denotes MOSFET noise factor.

3.4. RGC (Regulated Cascode) TIA

It utilizes local feedback technique as shown in figure 6 and gives gain on wider bandwidth scale but has high value of input inferred noise [17]. It has less input impedance and high output impedance. The local negative feedback within the RGC TIA (M3 & M4) boosts the trans-conductance of M1 by the value of the voltage gain of the common-source amplifier (M3 & M4).

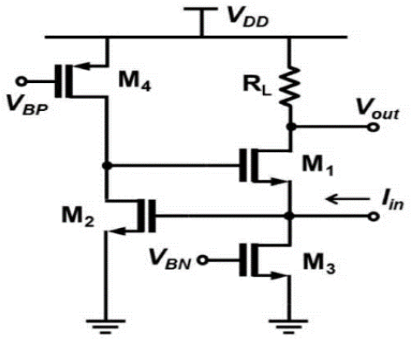

Figure 6: RGC TIA

- Gain $G = R_L$
- Bandwidth $BW = \frac{1}{g_{m1}g_{m2}C_p(r_{02}\|r_{04})}$
- Input referred noise current $\frac{4k_BT}{R_L} + 4k_BT\Upsilon g_{m3} + \frac{4k_BT\Upsilon(g_{m2}+g_{m4})}{g_{m2}^2}\omega^2 C_P^2$

3.5. TIA with capacitive feedback

In this topology input current is amplified and then is converted to voltage by R2 resistor has lesser input inferred noise and higher gain. But they are used only for low frequencies shown on figure 7 [18].

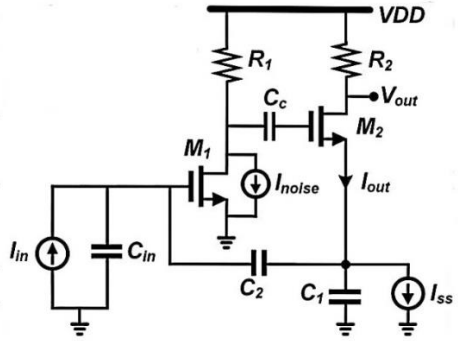

Figure 7: TIA with capacitive feedback

- Gain A= $R_L\left(1+\frac{C_2}{C_1}\right)$
- Bandwidth $BW = \sqrt{2}Ag_{m1}\frac{C_1}{C_2}(C_1 + C_P)$
- Input referred noise current $\frac{1}{\left(1+\frac{C_2}{C_1}\right)}\left(\frac{4k_BT}{R_L}+\frac{i_b^2}{\Delta f}\right)+\frac{v_n^2}{\Delta f}\omega^2\left(C_1+C_p\right)^2$

3.6. TIA with integrator and differentiator

The first stage is an integrator biased with a pseudo resistor RB giving a phase shift of 90°. The second stage is a differentiator formed by a series capacitor and a feedback resistor to compensate the

total feedback loop phase to 0°/180°. In this topology due to high impedance value given by RB, the capacitance ratio (C_2 /C_1) is reduced to increase gain and reduce noise shown in figure 8 [19].

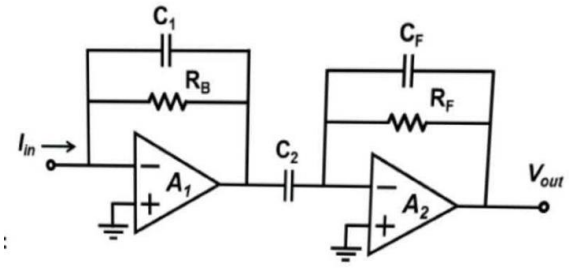

Figure 8: TIA with integrator and differentiator

- Gain $G = R_F \frac{C_2}{C_1}$
- Bandwidth $BW = \frac{1}{R_F C_F}$
- Input referred noise current $\frac{4k_BT}{R_B} + \frac{4k_BT}{R_f\left(\frac{C_2}{C_1}\right)^2} + \frac{v_n^2}{\Delta f}\omega^2\left(C_1 + C_p\right)^2$

3.7. Differential TIA

This topology is used due to its complementary results of the two different stage which tolerates interface to the following main amplifier stage as shown in figure 9. The differential configuration through the photo-receiver decreases the effect of bond wire inductance of ground and supply voltage by reducing concurrent switching currents. This trans-impedance amplifier is selected mutually with source having shunt feedback resistance and a resistive load. Its main use is to change the input current to an output voltage with a further rise in the gain of the amplifier [20].

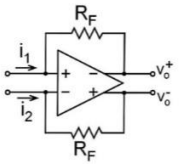

Figure 9: Differential TIA

- Gain $A_d = g_m\left(R_f \| \frac{R_L}{2}\right)$

3.8. Switched capacitor feedback TIA

The switched capacitor based trans-impedance amplifier shown in figure 10 has high accuracy, high linearity, CMOS integrated structure and is mostly used for Lab-on-chip type systems. They also offer desirable features such as low power and low noise [21].

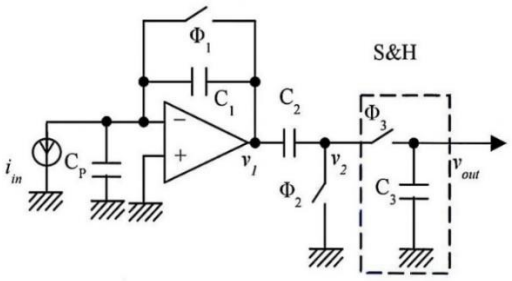

Figure 10: Switched Capacitor TIA

- Gain $G \approx \frac{T}{C_1}$ where T is the clock period.
- TIA output voltage at the completion of each T is $v_o(nT) = \frac{1}{C_1}\int_{t_2+T(n-1)}^{t_3+T(n-1)} i_{in}(t)\,dt$ where n is 1,2,3….

3.9. TIA with T-resistor feedback network

This topology overcomes the trade-off between gain and bandwidth which is a disadvantage in resistive feedback topology. It is possible to increase the bandwidth range here even after smaller values of R_f as shown in Fig. 11 but with an increased value of input inferred noise [22].

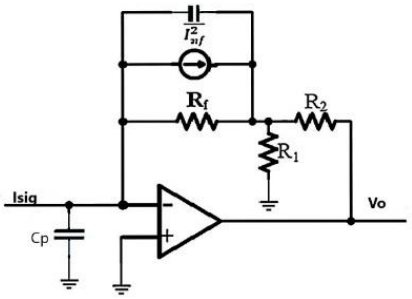

Figure 11: T-resistor feedback TIA

3.10. Inverter TIA

This topology consists of a PMOS and NMOS as shown in figure 12 with a pseudo-feedback resistor Rf. The transistor works in subthreshold region providing high gain bandwidth product with less power consumption. Its performance in terms of noise is also better [23].

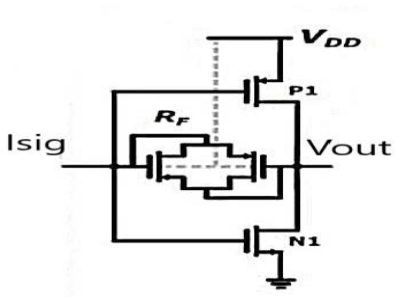

Figure 12: Inverter TIA

- Gain $G = -(g_{mn1} + g_{mp1})R_F$
- Input referred noise current $4k_BT\left[\frac{(2\pi fC_{PD})^2+(g_m)^2}{(1-g_mR_F)^2}R_F + 1 + \frac{(2\pi fC_{PD}R_F)^2}{(1-g_mR_F)^2}(g_{mn}\gamma_n + g_{mp}\gamma_p)\right]$

Table 1: Summary of various parameters of front end TIAs used in CMOS-MEMS Resonators

S.No.	Front-end TIAs topologies	TIA Gain	B/W	I/P referred noise current
1.	TIA with buffer and resistor as load	R_L	$\frac{1}{R_LC_P}$	$\frac{4k_BT}{R_L} + \frac{v_n^2}{\Delta f}\omega^2C_P^2$
2.	TIA with negative feedback (for $R_f << R_b$)	R_F	$\frac{\sqrt{2}}{R_FC_F}$	$\frac{4k_BT}{R_L} + \frac{v_n^2}{\Delta f}\left(\frac{1}{R_F^2} + \omega^2(C_P + C_F)^2\right)$
3.	TIA with negative feedback (for $R_f \rightarrow R_b$)	$\frac{1}{\omega C_F}$	$\frac{1}{R_BC_F}$	$\frac{4k_BT}{R_B} + \frac{v_n^2}{\Delta f}\left(\frac{1}{R_B^2} + \omega^2(C_P + C_F)^2\right)$
4.	TIA as current amplifier	NR_L	$\frac{1}{g_{m1}C_P}$	$4k_BT\Upsilon(g_{m1} + g_{m3}) + 4k_BT\left(\Upsilon g_{m2} + \frac{1}{R_2}\right)\frac{1}{N^2}$
5.	RGC (Regulated cascode) TIA	R_L	$\frac{1}{g_{m1}g_{m2}C_p(r_{02}\|\|r_{04})}$	$\frac{4k_BT}{R_L} + 4k_BT\Upsilon g_{m3} + \frac{4k_BT\Upsilon(g_{m2}+g_{m4})}{g_{m2}^2}\omega^2C_P^2$
6.	TIA with capacitive feedback	$R_L\left(1 + \frac{C_2}{C_1}\right)$	$\sqrt{2A}g_{m1}\frac{C_1}{C_2}(C_1 + C_P)$	$\frac{1}{\left(1+\frac{C_2}{C_1}\right)}\left(\frac{4k_BT}{R_L} + \frac{i_b^2}{\Delta f}\right) + \frac{v_n^2}{\Delta f}\omega^2(C_1 + C_p)^2$
7.	TIA with integrator and differentiator	$R_F\frac{C_2}{C_1}$	$\frac{1}{R_FC_F}$	$\frac{4k_BT}{R_B} + \frac{4k_BT}{R_f\left(\frac{C_2}{C_1}\right)^2} + \frac{v_n^2}{\Delta f}\omega^2(C_1 + C_p)^2$
8.	Inverter TIA	$-(g_{mn} + g_{mp})R_O$	$\frac{A_{INV}+1}{2\pi(R_O+R_F)C_{IN}}$	$4k_BT\left[\frac{(2\pi fC_{PD})^2+(g_m)^2}{(1-g_mR_F)^2}R_F + 1 + \frac{(2\pi fC_{PD}R_F)^2}{(1-g_mR_F)^2}(g_{mn}\gamma_n + g_{mp}\gamma_p)\right]$

4. Recent Developments

The author in [21] reported a dual probe STM (Scanning Tunnelling Microscopy) system fabricated using CMOS-MEMS technology with a switched capacitor TIA on single chip for each

probe. The tunnelling current is sensed and amplified by the TIA. Here imaging throughput of the STM is increased by multi-channel imaging and the TIA has low power consumption and lesser noise.

The author in [23] designed a dual frequency oscillator made of seesaw shaped tungsten resonator using BEOL (back ed of line) CMOS technology and ultra-compact TIA core. It was operated with reduced voltage supply and its phase noise at two different operating frequencies are noted and finally a comparative analysis with existing topologies were given.

The author in [24] proposed a back end of line embedded CMOS-MEMS resonator with a double ended tuning fork working in non-linear region and designed using standard 0.35µm CMOS process along with TIA with integrator and differentiator to find their figure of merit. The TIA has high gain and very less noise.

The author in [25] proposed a Lame mode MEMS resonator with TIA in fully differential configuration showing the performance of oscillator in terms of noise and stability. The TIA bandwidth can be configured to achieve minimum input referred noise current and frequency stability.

The author in [26] designed RGC-TIA for a MEMS oscillator to minimize its loading effect and also reducing the input parasitic capacitance of the TIA. A wine glass disk resonator is proposed using silicon carbide substrate operating in bulk mode. Here the RGC-TIA acts like a buffer and is so designed to minimize the input referred noise.

The author in [27] proposed a low power RGC-TIA and Cherry-Hooper wide band amplifier for VHF micromechanical systems. A linear RLC model is interfaced with this TIA for showing oscillations. The TIA gain and bandwidth are chosen to compensate the loss of resonator.

The author in [28] presented a tuneable gain front-end TIA integrated with CMOS-MEMS resonators with low power consumption and lesser noise. The system is analysed both in open loop and closed loop configuration. Here different resistances are used to achieve extremely low input current noise.

The author in [29] presented a monolithic MEMS oscillator with ultra-low power consumption fabricated with TIA on same die to get a higher Q value giving a comparative analysis with quartz crystal oscillators. Here capacitive TIA compensate the high insertion loss of the resonator keeping zero phase delay at operating frequency.

The author in [30] proposed a CMOS-MEMS oscillator with integrated TIA and analysed with piezoelectric crystal oscillators with ultra-low power specifications. Here optimization of input capacitance and thermal noise voltage of the amplifier is done by integrating the TIA with resonator.

The author in [31] presented a micromechanical active low pixel array with BEOL CMOS-MEMS structures and a power scalable TIA and analysed to obtain better phase noise for improving the frequency stability, the phase feedback noise suppression technique. This proposed TIA occupies less chip area in comparison to ID-TIA.

Table 2: Comparison of reported work

Reported work	TIA Gain	BW	O/P Voltage noise	I/P Referred current noise	CMOS Technology	Topology	Power consumption
[12]	330 kΩ-1.17 MΩ	50MHz	225nV/√Hz	192 fA/√Hz	0.35 µm	Capacitive feedback	930 µW
[21]	88 MΩ	40kHz	-	25fA/√Hz	0.35µm	Switched capacitor	3.2Mw

[23]	157dBΩ	1MHz	48.1nV/√Hz	0.67 fA/√Hz	0.35µm	Pseudo resistor feedback	8.5µW
[24]	7.94 MΩ	1.2MHz	199nV/√Hz	Less than 25 fA/√Hz	0.35 µm	Integrator-differentiator	150 µw
[25]	12.5kΩ-794 kΩ	90MHz	3.18µV/√Hz	14.5pA/√Hz	65 nm	Differential	900 µW
[26]	112.5dBΩ	239MHz	-	-	130nm	RGC	360µW
[27]	25kΩ-89kΩ	280 MHz	-	-	0.18 µm	RGC	1.57 mW
[28]	1.4MΩ-20MΩ	20MHz	-	32fA/√Hz	0.35µm	Differential	1.2mW
[29]	108.4MΩ	221kHz	-	2pA/√Hz	0.18µm	Capacitive feedback	1.69µW
[30]	148dBΩ	100MHz	126nV/√Hz	5fA/√Hz	0.35µm	Pseudo resistor feedback	300µW
[31]	127-150dBΩ	>10MHz	1.4 µV/√Hz	500fA/√Hz	0.35µm	Shunt-shunt feedback	30µW-2.85mW
[33]	88MΩ	1.5Hz-795kHz	1.5 µV/√Hz	3.1fA/√Hz	0.18µm	Two stage OTA with common feedback	561µW

5. Scope of Future Work

CMOS-MEMS resonators are designed and integrated using TIA for the purpose of size reduction, lower power consumption and fabrication on a single chip. NEMS (Nano electromechanical systems) are the mechanical structures in Nano-metres range and BIOTRONICS are the miniaturized hardware circuits or technologies involved in the life sciences these are some of the fields in which research is going on and still have large scope for future exploration along with silicon less CMOS-MEMS structures for a cheaper fabrication [32, 33].

6. Conclusion

In this paper various front-end TIA topologies are discussed which are used with CMOS-MEMS resonators using on- chip integration. These integrated structures occupy minimum chip area for fabrication and have longer life due to reduced power consumption. The use of TIA helps in amplifying the current signals obtained from the transducer by converting the light signals of the photodiode sensors. The selection of the TIA topology used directly depends on the phase noise and nonlinearities involved. The value of input inferred noise gives the phase noise and there is a trade-off between noise and bandwidth achieved. The deciding factor is the resonator frequency with which the TIA is used. Among all the topologies discussed above, the resistive feedback topology is the simplest one in configuration and gives the best performance in terms of low noise, better gain, and higher bandwidth trade-off.

7. References

[1] Atef, A., Atef, M., Khaled, E. E. M., & Abbas, M. (2020). CMOS transimpedance amplifiers for biomedical applications: A comparative study. *IEEE Circuits and Systems Magazine*, *20*(1), 12-31.

[2] Kamrani, E., & Sawan, M. (2011, November). Fully integrated CMOS avalanche photodiode and distributed-gain TIA for CW-fNIRS. In *2011 IEEE Biomedical Circuits and Systems Conference (BioCAS)* (pp. 317-320). IEEE.

[3] Costanzo, R., & Bowers, S. M. (2020). A 10-GHz bandwidth transimpedance amplifier with input DC photocurrent compensation loop. *IEEE Microwave and Wireless Components Letters*, *30*(7), 673-676.

[4] Wang, G., Atef, M., & Lian, Y. (2018). Towards a continuous non-invasive cuffless blood pressure monitoring system using PPG: Systems and circuits review. *IEEE Circuits and systems magazine*, *18*(3), 6-26.

[5] Kao, Y. H., Chao, P. C. P., & Wey, C. L. (2018). Towards maximizing the sensing accuracy of an cuffless, optical blood pressure sensor using a high-order front-end filter. *Microsystem Technologies*, *24*(11), 4621-4630.

[6] Kim, H. G., & Jee, D. W. (2017, September). A< 25 μW CMOS monolithic photoplethysmographic sensor with distributed 1b delta-sigma light-to-digital convertor. In *ESSCIRC 2017-43rd IEEE European Solid State Circuits Conference* (pp. 55-58). IEEE.

[7] Marefat, F., Erfani, R., Kilgore, K. L., & Mohseni, P. (2020). A 280 μW, 108 dB DR PPG-Readout IC With Reconfigurable, 2nd-Order, Incremental ΔΣM Front-End for Direct Light-to-Digital Conversion. *IEEE Transactions on Biomedical Circuits and Systems*, *14*(6), 1183-1194.

[8] Pribadi, E. F., Pandey, R. K., & Chao, P. C. P. (2021). Design and implementation of a new light to digital converter for the PPG sensor. *Microsystem Technologies*, *27*(6), 2461-2472.

[9] Kumar, S. (2021, April). A Review of Transimpedance Amplifiers Used in Biomedical Applications. In *2021 5th International Conference on Computing Methodologies and Communication (ICCMC)* (pp. 1314-1321). IEEE.

[10] Abdolvand, R., Bahreyni, B., Lee, J. E. Y., & Nabki, F. (2016). Micromachined resonators: A review. *Micromachines*, *7*(9), 160.

[11] Chen, C. Y., Li, M. H., & Li, S. S. (2018). CMOS-MEMS resonators and oscillators: A review. *Sensors Mater.*, *30*(4), 733-756.

[12] Perelló-Roig, R., Verd, J., Bota, S., & Segura, J. (2021). A Tunable-Gain Transimpedance Amplifier for CMOS-MEMS Resonators Characterization. *Micromachines*, *12*(1), 82.

[13] Uranga, A., Verd, J., & Barniol, N. (2015). CMOS–MEMS resonators: From devices to applications. *Microelectronic Engineering*, *132*, 58-73.

[14] Kamrani, E., Chaddad, A., Lesage, F., & Sawan, M. (2013, May). Integrated transimpedance amplifiers dedicated to low-noise and low-power biomedical applications. In *2013 29th Southern Biomedical Engineering Conference* (pp. 5-6). IEEE.

[15] Salvia, J., Lajevardi, P., Hekmat, M., & Murmann, B. (2009, September). A 56MΩ cmos tia for mems applications. In *2009 IEEE Custom Integrated Circuits Conference* (pp. 199-202). IEEE.

[16] Woo, J. K., Boyd, C., Cho, J., & Najafi, K. (2017, June). Ultra-low-noise transimpedance amplifier for high-performance MEMS resonant gyroscopes. In *2017 19th International Conference on Solid-State Sensors, Actuators and Microsystems (TRANSDUCERS)* (pp. 1006-1009). IEEE.

[17] Badal, M., Islam, T., Reaz, M. B. I., Yeng, L. S., Bhuiyan, M. A. S., & Haque, F. (2019). Advancement of CMOS transimpedance amplifier for optical receiver. *Transactions on Electrical and Electronic Materials*, *20*(2), 73-84.

[18] Rajabzadeh, M., Djekic, D., Haeberle, M., Becker, J., Anders, J., & Ortmanns, M. (2018, May). Comparison study of integrated potentiostats: Resistive-TIA, Capacitive-TIA, CT ΣΔ Modulator. In *2018 IEEE International Symposium on Circuits and Systems (ISCAS)* (pp. 1-5). IEEE.

[19] Singh, C. P., Pathania, A., Sharma, K., Madan, J., & Sharma, R. (2019, March). Design of an Integrator-Differentiator Block For a Transimpedance Amplifier Using $0.18\mu\mathrm {m} $ Technology. In *2019 Devices for Integrated Circuit (DevIC)* (pp. 394-397). IEEE.

[20] Royo, G., Garcia-Bosque, M., Sánchez-Azqueta, C., Aldea, C., Celma, S., & Gimeno, C. (2017, May). Transimpedance amplifier with programmable gain and bandwidth for capacitive MEMS accelerometers. In *2017 IEEE International Instrumentation and Measurement Technology Conference (I2MTC)* (pp. 1-5). IEEE.

[21] Tang, Y., Zhang, Y., Fedder, G. K., & Carley, L. R. (2012, October). An ultra-low noise switched capacitor transimpedance amplifier for parallel scanning tunneling microscopy. In *SENSORS, 2012 IEEE* (pp. 1-4). IEEE.

[22] Zhang, Y., Wang, J., Santhanam, S., & Fedder, G. K. (2011, June). Active CMOS-MEMS conductive probes and arrays for tunneling-based atomic-level surface imaging. In *2011 16th International Solid-State Sensors, Actuators and Microsystems Conference* (pp. 2446-2449). IEEE.

[23] Riverola, M., Sobreviela, G., Torres, F., Uranga, A., & Barniol, N. (2016). Single-resonator dual-frequency BEOL-embedded CMOS-MEMS oscillator with low-power and ultra-compact TIA core. *IEEE Electron Device Letters*, *38*(2), 273-276.

[24] Li, M. H., Chen, C. Y., Liu, C. Y., & Li, S. S. (2016). A Sub-150-$\mu\text {W} $ BEOL-Embedded CMOS-MEMS Oscillator With a 138-dB $\Omega $ Ultra-Low-Noise TIA. *IEEE Electron Device Letters*, *37*(5), 648-651.

[25] Bouchami, A., Elsayed, M. Y., & Nabki, F. (2019). A Sub-mW 18-MHz MEMS oscillator based on a 98-dBΩ adjustable bandwidth transimpedance amplifier and a Lamé-mode resonator. *Sensors*, *19*(12), 2680.

[26] Mekky, R. H., Cicek, P. V., & El-Gamal, M. N. (2013, December). Ultra low-power low-noise transimpedance amplifier for MEMS-based reference oscillators. In *2013 IEEE 20th International Conference on Electronics, Circuits, and Systems (ICECS)* (pp. 345-348). IEEE.

[27] Li, M. H., Li, C. S., Hou, L. J., Liu, Y. C., & Li, S. S. (2012, May). A 1.57 mW 99dBΩ CMOS transimpedance amplifier for VHF micromechanical reference oscillators. In *2012 IEEE International Symposium on Circuits and Systems (ISCAS)* (pp. 209-212). IEEE.

[28] Sobreviela, G., Uranga, A., & Barniol, N. (2014, June). Tunable transimpedance sustaining-amplifier for high impedance CMOS-MEMS resonators. In *2014 10th Conference on Ph. D. Research in Microelectronics and Electronics (PRIME)* (pp. 1-4). IEEE.

[29] Kuo, F. Y., Chang, C. F., & Wen, K. A. (2014, November). CMOS 0.18 μm standard process capacitive MEMS high-Q oscillator with ultra low-power TIA readout system. In *SENSORS, 2014 IEEE* (pp. 911-914). IEEE.

[30] Sobreviela, G., Riverola, M., Torres, F., Uranga, A., & Barniol, N. (2017, June). Ultra compact CMOS-MEMS oscillator based on a reliable metal-via MEMS resonators with noise-matched high-gain transimpedance CMOS amplifier. In *2017 19th International Conference on Solid-State Sensors, Actuators and Microsystems (TRANSDUCERS)* (pp. 1943-1946). IEEE.

[31] Bhosale, K., Chen, C. Y., Li, M. H., & Li, S. S. (2021, January). Standard CMOS Integrated Ultra- Compact Micromechanical Oscillating Active Pixel Arrays. In *2021 IEEE 34th International Conference on Micro Electro Mechanical Systems (MEMS)* (pp. 157-160). IEEE.

[32] Baltes, H., Brand, O., Hierlemann, A., Lange, D. A. L. D., & Hagleitner, C. A. H. C. (2002, January). CMOS MEMS-present and future. In *Technical Digest. MEMS 2002 IEEE International Conference. Fifteenth IEEE International Conference on Micro Electro Mechanical Systems (Cat. No. 02CH37266)* (pp. 459-466). IEEE.

[33] Serri, M., & Saeedi, S. (2020). Ultra-low-noise TIA topology for MEMS gyroscope readout. *AEU-International Journal of Electronics and Communications*, *118*, 153145.